Monthly Notices
of the
ROYAL ASTRONOMICAL SOCIETY

Mon. Not. R. Astron. Soc. **402,** 429–435 (2010) doi:10.1111/j.1365-2966.2009.15891.x

Metals, dust and the cosmic microwave background: fragmentation of high-redshift star-forming clouds

Raffaella Schneider[1]★ and Kazuyuki Omukai[2]

[1]*INAF/Osservatorio Astrofisico di Arcetri, Largo Enrico Fermi 5, 50125 Firenze, Italy*
[2]*National Astronomical Observatory of Japan, Mitaka, Tokyo 181-8588, Japan*

Accepted 2009 October 16. Received 2009 October 16; in original form 2009 September 8

ABSTRACT

We investigate the effects of the cosmic microwave background (CMB) radiation field on the collapse of pre-stellar clouds. Using a semi-analytic model to follow the thermal evolution of clouds with varying initial metallicities and dust contents at different redshifts, we study self-consistently the response of the mean Jeans mass at cloud fragmentation to metal line cooling, dust cooling and the CMB.

In the absence of dust grains, at redshifts $z \leq 10$ moderate characteristic masses (of tens of $M_\odot$) are formed when the metallicity is $10^{-4}\,Z_\odot \leq Z \leq 10^{-2.5}\,Z_\odot$; at higher metallicities, the CMB inhibits fragmentation and only very large masses (of approximately hundreds of $M_\odot$) are formed. These effects become even more dramatic at $z > 10$ and the fragmentation mass scales are always ≥hundreds of $M_\odot$, independent of the initial metallicity.

When dust grains are present, sub-solar mass fragments are formed at any redshift for metallicities $Z \geq 10^{-6}\,Z_\odot$ because dust cooling remains relatively insensitive to the presence of the CMB. When $Z > 10^{-3}\,Z_\odot$, heating of dust grains by the CMB at $z \geq 5$ favours the formation of larger masses, which become super-solar when $Z \geq 10^{-2}\,Z_\odot$ and $z \geq 10$. Finally, we discuss the implications of our result for the interpretation of the observed abundance patterns of very metal-poor stars in the Galactic halo.

Key words: stars: formation – stars: Population II – ISM: abundances – galaxies: evolution – cosmic microwave background.

1 INTRODUCTION

The origin of the stellar initial mass function (IMF) and its variation with cosmic time or with diverse environmental conditions still lack a complete physical interpretation. Observationally, the present-day stellar IMF appears to have an almost universal profile, characterized by a power law at large masses and flattening below a characteristic mass of $M_{\rm ch} \approx 1\,M_\odot$ with a plateau which extends down to the brown dwarf regime (see Chabrier 2003 and references therein). This mass scale, which represents the 'typical' outcome of the star formation process, appears to be remarkably uniform in diverse environments where the initial conditions for star formation can vary considerably (see Elmegreen, Klessen & Wilson 2008).

Among the many proposed explanations, the origin of the characteristic stellar mass and the broad peak of the IMF are best attributed to gravitational fragmentation, which sets the mean Jeans mass at cloud fragmentation (see Bonnell, Larson & Zinnecker 2007 for a comprehensive review):

$$M_{\rm frag} = \rho\lambda_{\rm J}^3 \sim 700\,M_\odot \left(\frac{T_{\rm frag}}{200\,{\rm K}}\right)^{3/2} \left(\frac{n_{\rm frag}}{10^4\,{\rm cm}^{-3}}\right)^{-1/2}, \quad (1)$$

where the Jeans length is defined as

$$\lambda_{\rm J} = \left(\frac{\pi kT}{\mu m_{\rm H} G\rho}\right)^{1/2}.$$

The process of gravitational fragmentation can be investigated using thermal physics within the framework of the classical Jeans criterion: fragmentation occurs at the end of an efficient cooling phase, when the temperature decreases for increasing density and the effective adiabatic index switches from $\gamma < 1$ to $\gamma > 1$ (the pressure $p \propto \rho^\gamma$, where ρ is the density); the typical fragmentation mass scale is given by the thermal Jeans mass at that epoch (Schneider et al. 2002; Larson 2005). The appearance of a characteristic mass at the inflection point in the equation of state has been also demonstrated numerically in 3D simulations by Jappsen et al. (2005), supporting the idea that the distribution of stellar masses depends mainly on the thermodynamical state of the star-forming gas.

In the physical conditions which apply to star-forming regions in the present-day Universe, the application of the above criterion leads

★E-mail: raffa@arcetri.astro.it

to a characteristic fragmentation mass of $M_{\rm frag} \sim 2\,{\rm M}_\odot$. About a half of this gas is expected to be ejected by a protostellar outflow without accreting (e.g. Matzner & McKee 2000).

If we apply the same criterion to primordial star-forming regions, we find a fragmentation mass of the order of $M_{\rm frag} \sim 700\,{\rm M}_\odot$, which corresponds to the Jeans mass at the temperature and density where cooling by molecular hydrogen becomes less efficient due to the non-local thermodynamic equilibrium (NLTE)–LTE transition in the level populations of the molecule. These clumps are the immediate progenitors of the stars, in agreement with the results found by 3D numerical simulations (Abel, Brian & Norman 2002; Bromm, Coppi & Larson 2002; Yoshida, Omukai & Hernquist 2008).

Thus, between the primordial and the present-day conditions there is a clear transition in fragmentation scales which is believed to be mainly driven by the progressive enrichment of star-forming clouds with metals (Bromm et al. 1999; Omukai 2000; Schneider et al. 2002; Bromm & Loeb 2003; Santoro & Shull 2006; Smith, Sigurdsson & Abel 2008) and dust grains (Schneider et al. 2003; Omukai et al. 2005; Tsuribe & Omukai 2006; Clark, Glover & Klessen 2008).

Note, however, that the presence of gas-phase metals cannot by itself lead to solar or sub-solar characteristic masses. In fact, metal line-cooling is efficient in the initial evolution of collapsing gas clouds, for densities in the range of 10^4–$10^6\,{\rm cm}^{-3}$, and induces fragmentation into relatively large clumps, with characteristic fragment masses of a few tens of ${\rm M}_\odot$ up to initial gas metallicities $Z \lesssim 10^{-2}\,{\rm Z}_\odot$ (Schneider et al. 2006). Conversely, the formation of solar or sub-solar mass fragments might operate already at metallicities $Z_{\rm cr} = 10^{-6}\,{\rm Z}_\odot$ in the presence of dust grains, which provide an efficient source of cooling at densities of $\gtrsim 10^{13}\,{\rm cm}^{-3}$. Since dust can be promptly synthesized in the ejecta of primordial supernovae (Todini & Ferrara 2001; Nozawa et al. 2003; Schneider, Ferrara & Salvaterra 2004; Bianchi & Schneider 2007), it is likely that its contribution to thermal and fragmentation history of collapsing clouds at high redshifts had been relevant.

An additional redshift-dependent effect is induced by the cosmic microwave background (CMB) which sets an effective temperature floor increasing with redshift. Clarke & Bromm (2003) have proposed a simple formula for the characteristic stellar mass which is identified by the Jeans mass fixed jointly by the gas temperature and the pressure set by the weight of the overlying baryons as the gas collapses in the parent dark matter halo. In this simple model, they do not follow the gas thermal evolution and the temperature is taken to be the maximum value between the CMB floor and either 200 K for H_2 cooling or 10 K for CO cooling. In the latter case, the characteristic stellar mass is set by the CMB temperature at all redshifts $z > 2.7$ and it is predicted to be $>10\,{\rm M}_\odot$ at $z > 10$.

The CMB influences the thermal evolution of collapsing gas clouds in two possible ways: (i) it affects the atomic and molecular line level populations and (ii) it heats the dust grains. In Omukai et al. (2005), we have estimated the impact of the CMB temperature floor at $z = 20$ on the evolution of pre-stellar clouds with varying initial metallicities. It was shown that the CMB affects the cloud evolution at low temperatures, which are reached for relatively large values of the initial metallicity, $Z > 10^{-3}\,{\rm Z}_\odot$.

Smith et al. (2009) have investigated the effects of the CMB on the collapse of pre-stellar clouds with varying initial metallicities by means of numerical simulations. They confirm that due to metal line-cooling, the gas becomes thermally coupled to the CMB for $Z > 10^{-2.5}\,{\rm Z}_\odot$ early in the evolution of the clouds when the density is still low. Note that a similar effect has been recently found by Jappsen et al. (2009) using 3D simulations starting from different initial conditions, namely protogalaxies forming within a previously ionized H II region that has not yet had time to cool and recombine. Even in the latter models, the gas cools rapidly to the CMB floor and no fragmentation occurs during the collapse for metallicities as high as $0.1\,{\rm Z}_\odot$.

Smith et al. (2009) conclude that the CMB inhibits fragmentation at large metallicities and that there were three distinct modes of star formation at high redshift: a primordial, producing very massive stars at very low metallicities ($Z < 10^{-3.75}\,{\rm Z}_\odot$); a CMB-regulated mode, producing moderate mass (tens of ${\rm M}_\odot$) stars at high metallicities ($Z > 10^{-2.5}\,{\rm Z}_\odot$ at redshift $z \sim 15$–20); and a low-mass (a few ${\rm M}_\odot$) mode existing between these two metallicities. As the Universe ages and the CMB temperature decreases, the range of the low-mass mode extends to higher metallicities, eventually becoming the only mode of star formation.

In their simulations, however, Smith et al. (2009) consider the thermal evolution in the presence of molecular coolants (H_2 and HD) and gas-phase metals only. They do not include H_2 formation heating, which affects the thermal evolution at moderate densities of $\geq 10^8\,{\rm cm}^{-3}$ in the primordial gas and at lower densities in the metal-enriched gas. Moreover, they do not take into consideration the possible presence of dust grains which significantly affect the gas thermal evolution even at very low metallicities via cooling by thermal emission and efficient H_2 formation on their surfaces (Schneider et al. 2003; Omukai et al. 2005; Schneider et al. 2006).

From an observational point of view, the number and properties of very metal-poor (VMP) stars in the Galactic halo with [Fe/H] <-2 seem to require a higher characteristic stellar mass in the past, with a redshift modulation consistent with that expected by the CMB (Hernandez & Ferrara 2001). Recent analyses of the surface elemental composition of VMP halo stars (Cayrel et al. 2004) show that the observed abundance pattern appears consistent with the predicted yields of Pop III stars with a characteristic mass of $\approx 10\,{\rm M}_\odot$ (Heger & Woosley 2008). Similar conclusions have been derived analysing the fraction of carbon-enhanced metal-poor stars (CEMP; Komiya et al. 2007; Tumlinson 2007). CEMP stars are a subset of metal-poor stars that show enhanced carbon-to-iron abundances ([C/Fe] > 1; Beers & Christlieb 2005). These stars are thought to be metal-poor low-mass stars ($<0.8\,{\rm M}_\odot$) that have acquired C enhancements at their convective surfaces by capturing the C-rich ejecta of an asymptotic giant branch (AGB) companion ($1.5\,{\rm M}_\odot < M_\star < 8\,{\rm M}_\odot$). Because the binary system that produces a CEMP star requires both a low-mass star and an intermediate-mass star, the incidence and chemical abundance signatures of CEMP stars reflect the underlying IMF in the range $1\,{\rm M}_\odot < M_\star < 8\,{\rm M}_\odot$ (Lucatello et al. 2005; Komiya et al. 2007; Tumlinson 2007).

On the basis of these considerations, Tumlinson (2007) suggests that the CMB is shaping the characteristic mass of the IMF and proposes the following parametrization:

$$M_{\rm ch}/{\rm M}_\odot = 1.06\,{\rm M}_\odot \left(\frac{\max[(1+z)2.73\,{\rm K}, 8\,{\rm K}]}{10\,{\rm K}} \right)^{1.7}, \qquad (2)$$

which implies that $M_{\rm ch} = 0.72$, 6.87 and $20.63\,{\rm M}_\odot$ at $z = 0$, 10 and 20, respectively.

The question is whether this observationally motivated CMB-regulated IMF can be reconciled with theoretical models for the thermal evolution and fragmentation of star-forming clouds at very low metallicities.

Here we intend to revisit the role of the CMB in the evolution of protostellar clouds investigating in a self-consistent way the response of the fragmentation mass scale to metal line-cooling, dust cooling and the CMB.

The paper is organized as follows. In Section 2 we present the model adopted to follow the thermal and chemical evolution of collapsing protostellar clouds, in Section 3 we illustrate the main results of the analysis and in Section 4 we discuss their implications.

2 THE MODEL

The thermal and chemical evolution of star-forming gas clouds is studied using the model developed by Omukai (2000) and improved in Omukai et al. (2005). The collapsing gas clouds are described by a one-zone approach where all physical quantities are evaluated at the centre as a function of the central density of hydrogen nuclei, $n_{\rm H}$. The temperature evolution is computed by solving the energy equation

$$\frac{{\rm d}e}{{\rm d}t} = -p\,\frac{\rm d}{{\rm d}t}\,\frac{1}{\rho} - \Lambda_{\rm net}, \tag{3}$$

where the pressure, p, and the specific thermal energy, e, are given by

$$p = \frac{\rho k T}{\mu m_{\rm H}}, \tag{4}$$

$$e = \frac{1}{\gamma_{\rm ad} - 1}\,\frac{kT}{\mu m_{\rm H}}, \tag{5}$$

and ρ is the central density, T is the temperature, $\gamma_{\rm ad}$ is the adiabatic exponent, μ is the mean molecular weight and $m_{\rm H}$ is the mass of hydrogen nuclei. The terms on the right-hand side of the energy equation are the compressional heating rate,

$$\frac{{\rm d}\rho}{{\rm d}t} = \frac{\rho}{t_{\rm ff}} \qquad \text{with} \qquad t_{\rm ff} = \sqrt{\frac{3\pi}{32 G \rho}}, \tag{6}$$

and the net cooling rate, $\Lambda_{\rm net}$, which consists of three components:

$$\Lambda_{\rm net} = \Lambda_{\rm line} + \Lambda_{\rm cont} + \Lambda_{\rm chem}. \tag{7}$$

The first component, $\Lambda_{\rm line}$, represents the cooling rate due to the emission of line radiation, which includes molecular line emission of H_2, HD, OH, H_2O and CO, and atomic fine-structure line emission of C I, C II and O I. Following Omukai et al. (2005), H_2 collisional transition rates and HD parameters are taken from Galli & Palla (1998). The second component, $\Lambda_{\rm cont}$, represents the cooling rate due to the emission of continuum radiation, which includes thermal emission by dust grains and H_2 collision-induced emission. The last term, $\Lambda_{\rm chem}$, indicates the cooling/heating rate due to chemical reactions. When the gas cloud is optically thick to a specific cooling radiation, the cooling rate is correspondingly reduced by multiplying by the photon escape probability. Unless otherwise stated, the treatments of these processes are the same as in Omukai et al. (2005), to which we refer the interested reader for further details.

In particular, we adopt the reduced chemical model for low-metallicity clouds described in section 3.2 of Omukai et al. (2005). This model reproduces the temperature evolution and the abundances of the dominant chemical species following a network of 54 reactions (instead of the full 500 reactions of the original model) for 26 species (instead of 50).

In the present analysis, we are interested in investigating the effects of the CMB in the thermal evolution of the clouds at different metallicities. The CMB enters in our model in two ways: first through the level population of atomic/molecular lines and second through the heating of dust grains. These effects prevent the gas and dust temperature from falling below the radiation temperature. In addition, the higher dust temperature reduces the H_2 formation rate by surface reactions. The former effect is included in calculating the level populations of atomic and molecular species as in Omukai (2001, see appendix B). The latter effects are included through the energy-balance equation of grains:

$$4\,\sigma\,T_{\rm gr}^4\,\kappa_{\rm gr} = \Lambda_{\rm gas\rightarrow dust} + 4\,\sigma\,T_{\rm rad}^4\,\kappa_{\rm gr}, \tag{8}$$

where the left-hand side is the cooling rate of grains and the right-hand side is the heating rate by collisions with gas particles and by the CMB (see Omukai et al. 2005), and we have made the approximation that the Planck mean opacity for absorption is the same as for emission.

For gas at solar metallicity, the abundances of carbon and oxygen are $y_{\rm C} = 0.927 \times 10^{-4}$ and $y_{\rm O} = 3.568 \times 10^{-4}$, respectively. The mass fraction of dust grains is 0.939×10^{-2} below the water–ice evaporation temperature, and it decreases for higher temperatures as each grain component evaporates (Pollack et al. 1994). For lower metallicity gas, these values are reduced proportionally and we denote the corresponding abundances relative to the solar value as $[{\rm M/H}] = \log_{10}(Z/Z_\odot)$. Strictly speaking, we do not expect the regions enriched by the first supernovae to have a solar abundance pattern and the same dust grains present in the local neighbourhood. Yet, a more detailed analysis which self-consistently accounts for the elemental abundances and dust grain properties produced by metal-free supernovae with masses of 12–30 and 140–260 $M_\odot$ shows that the thermal evolution of protostellar clouds is qualitatively the same (see Schneider et al. 2006).

3 RESULTS

In this section, we discuss the model predictions for the thermal evolution of low-metallicity protostellar clouds at different redshifts, i.e. exposed to a CMB radiation field at different temperatures. We then discuss the resulting characteristic fragmentation mass scales.

3.1 Thermal evolution

In Fig. 1, we show the thermal evolution of collapsing protostellar clouds as a function of the central gas number density. The temperature divided by the mean molecular weight T/μ is shown as its variation with density is directly related to the effective adiabatic index $\gamma - 1 = {\rm d}\ln(T/\mu)/{\rm d}\ln n_{\rm H}$. Each panel represents the evolution for a specific initial metallicity, ranging from $[{\rm M/H}] = -5$(top left) to $[{\rm M/H}] = -1$ (bottom right). For each metallicity, we have explored the variation with redshift and the different curves in each panel represent clouds collapsing at $z = 0$ (solid), 5 (dotted), 10 (short dashed), 20 (long dashed) and 30 (dot–dashed). Thus, the effects of the CMB can be quantified by the deviations of the curves from the reference solid curve because at $z = 0$ the CMB temperature is too low to have any appreciable consequence on the clouds' thermal evolution.

As expected, the effects of the CMB increase with redshift (i.e. higher radiation temperature) and metallicity (i.e. lower gas temperature). However, even at metallicities as small as $[{\rm M/H}] = -5$, the thermal evolution at $z = 30$ shows deviations from the $z = 0$ track, despite the fact that at this low metallicity the gas temperature is higher than the CMB value. The deviation is caused by the suppression of H_2 formation on dust grains due to the increased dust temperature, which is almost equal to the CMB temperature. The

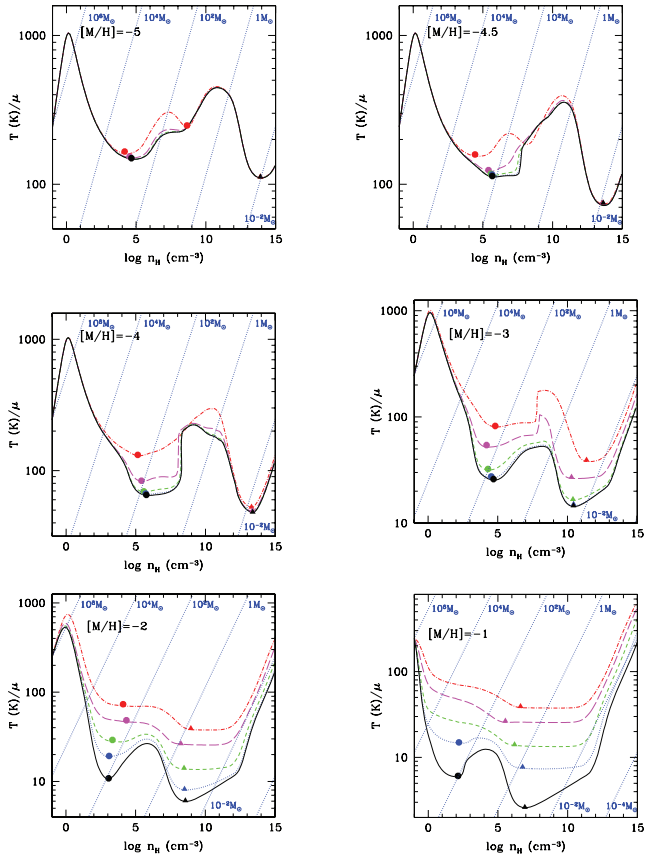

Figure 1. Thermal evolution as a function of the central gas number density for protostellar clouds with initial metallicities [M/H] = −5, −4.5, −3, −2, −1 (from the top left to the bottom right). The temperature divided by mean molecular weight is shown. For our assumed helium abundance ($y_{\rm He} = 0.0833$), the mean molecular weight changes from $\mu = 1.23$ (fully atomic hydrogen) to 2.29 (fully H_2). In each panel, the different curves correspond to the evolution of clouds at $z = 0$ (solid), 5 (dotted), 10 (short dashed), 20 (long dashed), and 30 (dot–dashed). The points identify the epochs of fragmentation induced by line cooling (dots) and dust cooling (triangles). The diagonal dotted lines identify the values of the Jeans masses corresponding to the given thermal states.

H_2 formation rate coefficient on dust grains is expressed as (Tielens & Hollenbach 1985)

$$k_{\rm H_2,gr} = \frac{6\times10^{-17}{\rm cm^3 s^{-1}}(T/300\,{\rm K})^{1/2}(Z/{\rm Z_\odot})f_{\rm a}}{1+4\times10^{-2}(T+T_{\rm gr})^{1/2}+2\times10^{-3}T+8\times10^{-6}T^2},$$

with

$$f_{\rm a} = \frac{1}{1+\exp[7.5\times10^2(1/75-1/T_{\rm gr})]}.$$

Thus, when $T_{\rm gr} \gtrsim 75$ K, $f_{\rm a}$ becomes very small. If the H_2 formation rate is not reduced at high dust temperatures, as suggested by Cazaux & Tielens (2004), the dependence of the thermal evolution on the CMB at these low metallicities would disappear.

For initial metallicities [M/H] < −3, the effects of the CMB on the cloud thermal evolution are limited to densities $n_{\rm H} < 10^8$ cm^{-3}, in the regime where line cooling dominates. At higher metallicities, the minimum temperature induced by dust cooling reaches the CMB value. Thus, the deviations from the $z = 0$ track are more pronounced and are present at all densities $n_{\rm H} \geq 10^3$ cm^{-3}, up to the regime where cooling is dominated by dust grains. Note that at [M/H] ≥ −2 and $z \gtrsim 20$, a decrease in T/μ beyond the point where the temperature reaches the CMB floor is due to the increase in μ as a result of H_2 formation.

In each panel, the points identify the epochs of fragmentation induced by line cooling (dots) and dust cooling (triangles), while the diagonal dotted lines represent some indicative values of the Jeans mass corresponding to the thermal states. As expected on the basis of arguments given in Section 1, the fragmentation epochs correspond to the inflection points of the equation of state.

More quantitatively, we identify the fragmentation epochs by the condition that the adiabatic index becomes $\gamma > 0.97$ after a phase of cooling (where $\gamma \ll 1$). The choice of a threshold value slightly smaller than unity is motivated by the fact that when the gas reaches the CMB temperature, γ may approach unity asymptotically, but never exceeds it. As an additional condition for fragmentation, we impose that $\gamma < 0.8$ during the cooling phase preceding the fragmentation epoch: this is to eliminate 'false' fragmentation points where γ is less than 1 only for a short period of time. The evolution of the adiabatic index γ as a function of the central number density for the same set of models shown in Fig. 1 is shown in Fig. 2.

For all but the lowest (highest) metallicity models, the two fragmentation phases (line-induced, at low densities and dust-induced at high-densities) are preserved even in the presence of the CMB. When [M/H] = −5 and $z = 30$, however, there appears to be an intermediate fragmentation phase which is due to H_2O cooling at densities of 10^7–10^8 cm^{-3}. At lower redshifts/higher metallicities, this phase is no longer present because at these intermediate densities the temperature is already too low (due to H_2/metal line-cooling) for H_2O cooling to have any appreciable effect. However, as can be inferred from the behaviour of the dot–dashed line in the top panel of Fig. 2, the intermediate fragmentation phase is most probably artificial as it depends very much on the fragmentation condition. With a stricter condition on the duration of the cooling phase, such as $\gamma < 0.7$, it would not be classified as a fragmentation phase.

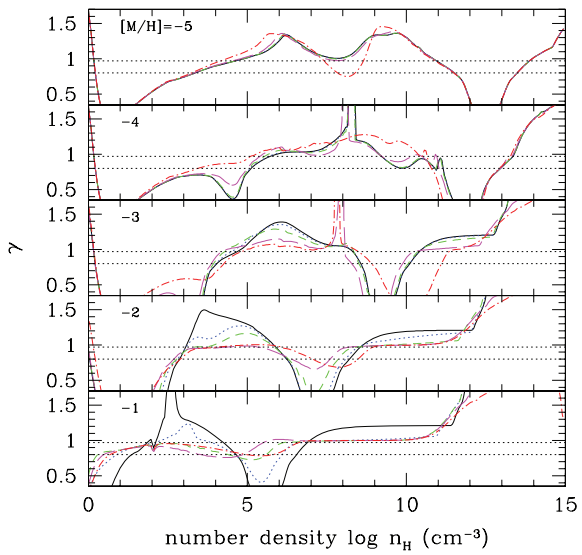

Figure 2. Evolution of the adiabatic index γ for clouds with initial metallicities [M/H] = −5, −4, −3, −2, −1 (from top to bottom). In each panel, the different curves show the evolution for a fixed metallicity and redshift $z = 0$ (solid), 5 (dotted), 10 (short dashed), 20 (long dashed) and 30 (dot–dashed). The horizontal dotted lines indicate the values limiting the fragmentation epoch, i.e. a cooling phase with $\gamma < 0.8$ followed by the condition that $\gamma > 0.97$ (see text).

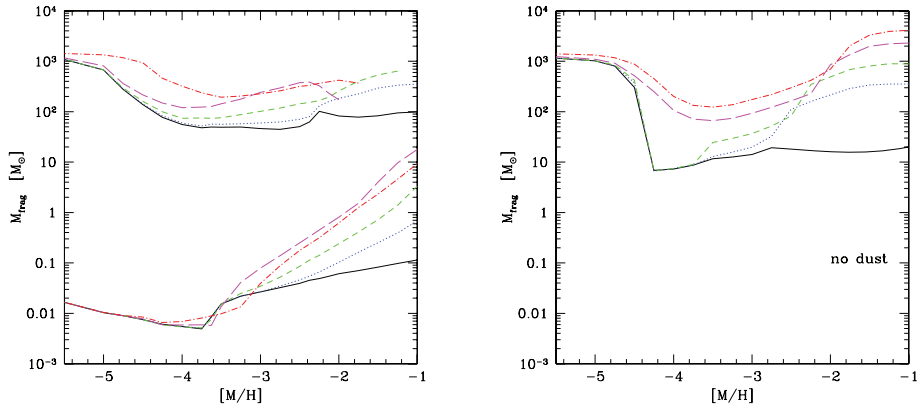

Figure 3. Characteristic fragmentation mass as a function of metallicity for $z = 0$ (solid), 5 (dotted), 10 (short dashed), 20 (long dashed) and 30 (dot–dashed). The left-hand panel shows the same set of models presented in Fig. 1 with the lower (upper) branch representing the masses associated with dust- (metal-) induced fragmentation. The right-hand panel illustrates a test model with no dust.

Finally, as can be inferred from the bottom panels of Figs 1 and 2, when [M/H] > -2 and $z \geq 10$, the line-induced and dust-induced fragmentation phases merge and the thermal evolution is controlled by the CMB temperature.

3.2 Fragmentation mass

In the present context, where we assume that thermal pressure is the main force opposing gravity, the characteristic mass of each fragment is given by the Jeans mass at the fragmentation epoch, given in equation (1). Fig. 3 shows the fragmentation masses as a function of metallicity and redshift. In the left-hand panel, the upper and lower branches are associated with line-induced and dust-induced fragmentation, respectively. Since line-induced fragmentation occurs at relatively low densities, the corresponding fragment masses are large. In particular, at the lowest metallicities we find that, at any redshift, the characteristic fragmentation mass scale, induced by H_2 line cooling, is $M_{\rm frag} \sim 10^3\,{\rm M}_\odot$, consistent with the results of numerical models. Still, even for metallicities in the range $-5 \leq [M/H] \leq -2$, metal line-cooling leads to fragment masses $M_{\rm frag} \geq 50\,{\rm M}_\odot$ (Schneider et al. 2006). Dust-induced fragmentation, which occurs at much higher densities, leads to significantly lower mass scales.

The CMB affects the amplitude of the characteristic mass in both line- and dust-induced phases. At any metallicity in the range $-5 \leq$ [M/H] ≤ -1, the presence of the CMB leads to larger characteristic masses in the line-induced phase, with a deviation from the reference $z = 0$ track which increases with metallicity and redshift. Even for clouds with metallicity [M/H] $= -4$, the characteristic mass is more than a factor of 2 larger at $z \geq 20$. As has already been discussed, the main effect of the CMB at these low metallicities is the suppression of H_2 formation on dust grains. In the dust-induced phase, instead, the effects of the CMB on the characteristic mass start to be appreciable only when the metallicity is [M/H] ≥ -3, when the temperature dip due to dust cooling hits the CMB floor. At [M/H] $= -3$, the deviation of the characteristic mass from the $z = 0$ track is by more than a factor of 2 at $z \geq 20$. At the highest metallicity considered in this analysis, [M/H] $= -1$, the characteristic mass in the line- (dust-) induced fragmentation is 100 (0.1), 350 (0.7), 640 (3.3) $\,{\rm M}_\odot$ at $z = 0$, 5, 10, respectively. At $z \geq 20$, it is no longer possible to discriminate between the two fragmentation phases (this is why the long dashed and dot–dashed lines in the upper branch are interrupted) and the fragmentation masses are $\approx 10\,{\rm M}_\odot$.

The above results are therefore consistent with the general trend suggested by Smith et al. (2009) that the characteristic fragment mass $M_{\rm frag}$ is first high, then it decreases and then it is again high (three modes) but in our analysis this trend is much less pronounced. To better compare with their analysis, we have run a set of test models with no dust and the characteristic masses in the line-induced fragmentation branch as a function of metallicity and redshift are shown in the right-hand panel of Fig. 3.

Since the total metallicity is the same in models with and without dust, about a factor of 3 more metals are present in the gas phase in the no-dust cases. At $z = 0$, $M_{\rm frag} \approx 1000\,{\rm M}_\odot$ when the metallicity is [M/H] < -4 and $M_{\rm frag} \approx 10\,{\rm M}_\odot$ above this threshold. At $z \leq 10$, the CMB starts to affect the characteristic mass when [M/H] ≥ -3.5, increasing it to several tens (hundreds) of $\,{\rm M}_\odot$ when [M/H] $= -3$ (≥ -2). At higher redshifts, the characteristic fragment masses are $\approx 1000\,{\rm M}_\odot$ when [M/H] < -4 and [M/H] > -2 but never decrease below $100\,{\rm M}_\odot$ in the intermediate range $-4 \leq$ [M/H] ≤ -2. Therefore, our analysis confirms that the CMB inhibits fragmentation at large metallicities but, in the absence of dust grains, we do not find any metallicity/redshift range where fragments of a few $\,{\rm M}_\odot$ can form. As already pointed out in Section 1, in their simulation Smith et al. (2009) do not consider H_2 formation heating nor H_2 formation on dust grains which may explain why they tend to find smaller fragment masses in the intermediate metallicity range. Also note that their model includes more atomic species than just C and O, such as Fe, Si and S, which provide additional cooling.

4 CONCLUSIONS

In this paper we have investigated the dependence of thermal and fragmentation properties of star-forming clouds on the environmental conditions, focussing on the interplay between metals, dust grains and the CMB at different redshifts.

Our results, based on an extended grid of models with varying initial metallicities and redshifts, can be summarized as follows.

(i) In the absence of dust grains, when fragmentation occurs at the end of the line-cooling phase, moderate characteristic masses (of tens of $\,{\rm M}_\odot$) are formed at redshifts $z \leq 10$ when the metallicity is $10^{-4}\,{\rm Z}_\odot \leq Z \leq 10^{-2.5}\,{\rm Z}_\odot$; at lower metallicities, the clouds follow the primordial fragmentation mode and at higher metallicity,

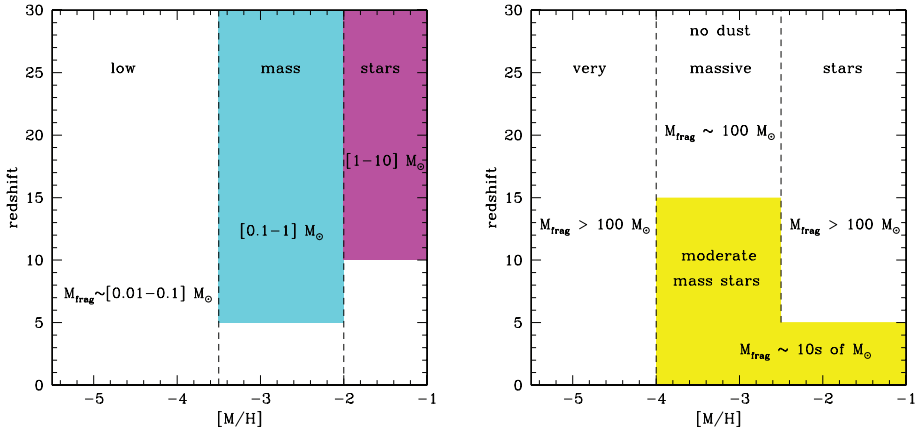

Figure 4. Schematic representation of the characteristic masses associated with the relevant fragmentation regimes in the metallicity–redshift plane. In the left-hand panel, we report only the typical scales associated with dust-induced fragmentation, since line-induced fragmentation leads to masses of $>50\,M_\odot$ independent of the initial metallicity or redshift. In the right-hand panel, we show the scales expected in models with no dust (see text).

$Z > 10^{-2.5}\,Z_\odot$, the CMB inhibits fragmentation and only very large masses, approximately hundreds of $M_\odot$, are formed. These effects become even more dramatic at $z > 10$, when the fragmentation mass scales are always $\geq$hundreds of $M_\odot$, independent of the initial metallicity.

(ii) When dust grains are present, at $z = 0$ two regimes are present: the line-induced fragmentation mode, which leads to fragment masses of $>50\,M_\odot$ at any metallicity, and the dust-induced fragmentation mode, which occurs at higher densities and leads to sub-solar mass fragments when $Z \geq 10^{-6}\,Z_\odot$. The effects of the CMB at $z > 0$ are important in both physical regimes: at very low metallicities, $Z < 10^{-4}\,Z_\odot$, line cooling becomes less efficient because of the suppression of H_2 formation on dust grains when the grain temperature becomes $\geq$75 K, at $z > 20$. At higher metallicities, metal line-cooling causes the gas to thermally couple with the CMB and the resulting fragments are very massive, with $M_{\rm frag} > 100\,M_\odot$ for $z \geq 5$. Dust cooling remains relatively insensitive to the presence of the CMB up to metallicities of $Z \sim 10^{-3}\,Z_\odot$ and sub-solar mass fragments are formed at any redshift. Above this threshold, heating of dust grains by the CMB at $z \geq 5$ favours the formation of larger masses, which become super-solar when $Z \geq 10^{-2}\,Z_\odot$ and $z \geq 10$.

(iii) Clouds enriched by metals and dust grains with a total metallicity $Z \geq 10^{-1}\,Z_\odot$ collapsing at $z > 5$ experience only a single fragmentation epoch (line-induced and dust-induced phases merge) and the characteristic masses are controlled by the CMB temperature, with $M_{\rm frag} = 0.5,\ 3,\ 20\,M_\odot$ for $z = 10,\ 20,\ 30$, respectively.

The characteristic fragmentation masses are schematically summarized in Fig. 4, where we report the typical scales associated with dust-induced fragmentation (left-hand panel) and in the absence of dust (right-hand panel) in the different redshift–metallicity regimes discussed above. We have not considered the fragmentation masses associated with line cooling in the models with dust as they are always $>50\,M_\odot$ independent of the initial metallicity and redshift (see the upper branch in the left-hand panel of Fig. 3).

Our results confirm the general trend suggested by previous semi-analytic (Omukai et al. 2005) and numerical models (Smith et al. 2009) that the CMB tends to inhibit fragmentation of relatively metal-enriched clouds collapsing at high redshift. However, the interplay between metals, dust and the CMB generates a complex dependence of the fragmentation mass on environmental conditions.

It is important to stress that in order to explore the observational consequences of such an environmental dependence, it would be necessary to infer the variation of the functional form of the IMF and not only of the characteristic mass. This issue has been recently addressed by Clark et al. (2009) who predict that, in star-forming regions with $Z > 10^{-5}\,Z_\odot$, competitive accretion can provide a natural explanation for the power-law form of the IMF, which is observed to be remarkably uniform in a wide variety of environments. The competitive accretion of gas from a common reservoir by a collection of protostellar cores requires that the characteristic fragmentation mass be much smaller than the mass of the cooling gas available. As a consequence, Clark et al. (2009) suggest that there may be a link between the CMB and the slope of the IMF and that in the absence of dust competitive accretion will not occur in regions with metallicities $Z \geq 10^{-3.5}\,Z_\odot$ collapsing at high redshift whereas it will occur at all redshifts and metallicities if dust cooling can operate.

As we have mentioned in Section 1, one of the main motivation for the present study was to assess whether the CMB could be a viable way to modulate the stellar IMF with redshift as suggested by recent analyses of the elemental abundances of VMP and CEMP stars (Komiya et al. 2007; Tumlinson 2007; Heger & Woosley 2008). In Fig. 5 we show the redshift dependence of the fragmentation mass scales found in the present analysis selecting only the parameter space which is compatible with fragment masses in the range $M_{\rm frag} \leq 10\,M_\odot$ in the presence of dust grains. As a comparison, the thin dotted line shows the empirical dependence of the characteristic stellar mass on redshift proposed by Tumlinson (2007, see equation 1). It is important to stress that the relation between the fragmentation mass scale and characteristic mass shaping the stellar IMF is not straightforward and several processes, such as competitive accretion or dynamical encounters, can act to make it not monotonic. However, the inspection of Fig. 5 suggests that for all but the highest metallicity, the redshift dependence predicted by our analysis is generally shallower than what is inferred from the empirical IMF. Moreover, observations indicate that the fraction of CEMP stars decreases with metallicity being 100 per cent at [Fe/H] < -4.5, $\sim$40 per cent at [Fe/H] < -3.5 and $\sim$20 per cent at [Fe/H] < -2 (Beers & Christlieb 2005). If CEMP stars reflect the

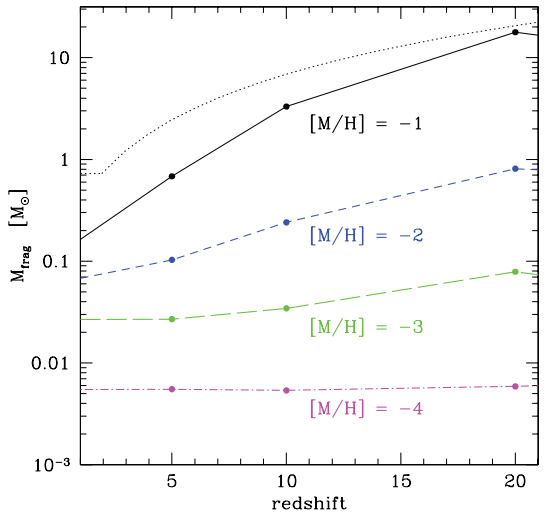

Figure 5. Redshift evolution of the fragmentation mass $M_{\rm frag}$ for clouds with initial metallicities [M/H] = −4, −3, −2, −1 (from bottom to top). The thin dotted line shows the empirical dependence of the stellar characteristic mass on the CMB temperature proposed by Tumlinson (2007, see text).

underlying IMF in the range $1\,{\rm M}_\odot < M < 8\,{\rm M}_\odot$, our results seem to indicate an opposite trend: the effects of the CMB on the characteristic mass increase with metallicity, suggesting that the CMB cannot be the only physical driver for the required modulation of the stellar characteristic mass.

ACKNOWLEDGMENTS

We are grateful to the referee, Simon Glover, for his careful reading of the manuscript which has helped us to improve the quality of the paper. We thank Andrea Ferrara and Stefania Salvadori for useful comments. RS acknowledges the support and hospitality of the National Astronomical Observatory of Japan.

REFERENCES

Abel T., Brian G., Norman M. L., 2002, Sci, 295, 93
Bianchi S., Schneider R., 2007, MNRAS, 378, 973
Beers T. C., Christlieb N., 2005, ARA&A, 43, 531
Bonnell I. A., Larson R. B., Zinnecker H., 2007, in Reipurth B., Jewitt D., Keil K., eds, Protostars and Planets V. Univ. of Arizona Press, Tucson, p. 149
Bromm V., Loeb A., 2003, Nat, 425, 812
Bromm V., Ferrara A., Coppi P., Larson R. B., 1999, MNRAS, 328, 969
Bromm V., Coppi P., Larson R. B., 2002, ApJ, 564, 23
Cayrel R. et al., 2004, A&A, 416, 1117
Cazaux S., Tielens A. G. G. M., 2004, ApJ, 604, 222
Chabrier G., 2003, ApJ, 586, L133
Clarke C. J., Bromm V., 2003, MNRAS, 343, 1124
Clark P. C., Glover S. C. O., Klessen R. S., 2008, ApJ, 672, 757
Clark P. C., Glover S. C. O., Bonnell I. A., Klessen R. S., 2009, ApJ, submitted (arXiv:0904.3302)
Elmegreen B. G., Klessen R. S., Wilson C. D., 2008, ApJ, 681, 365
Galli D., Palla F., 1998, A&A, 335, 403
Heger A., Woosley S. E., 2008, ApJ, submitted (arXiv:0803.3161)
Hernandez X., Ferrara A., 2001, MNRAS, 324, 484
Jappsen A. K., Klessen R. S., Larson R. B., Li Y., Mac Low M. M., 2005, A&A, 435, 611
Jappsen A. K., Mac Low M. M., Glover S. C. O., Klessen R. S., Kitsionas S., 2009, ApJ, 694, 1161
Komiya Y., Suda T., Minaguchi H., Shigeyama T., Aoki W., Fujimoto M. Y., 2007, ApJ, 658, 367
Larson R. B., 2005, MNRAS, 359, 211
Lucatello S., Gratton R. G., Beers T. C., Carretta E., 2005, ApJ, 625, 833
Matzner C. D., McKee C. F., 2000, ApJ, 545, 364
Nozawa T., Kozasa T., Umeda H., Maeda K., Nomoto K., 2003, ApJ, 598, 785
Omukai K., 2000, ApJ, 534, 809
Omukai K., 2001, ApJ, 546, 635
Omukai K., Tsuribe T., Schneider R., Ferrara A., 2005, ApJ, 626, 627
Pollack J. B., Hollenbach D., Beckwith S., Simonelli D. P., Roush T., Fong W., 1994, ApJ, 421, 615
Santoro F., Shull M. J., 2006, ApJ, 643, 26
Schneider R., Ferrara A., Natarajan P., Omukai K., 2002, ApJ, 571, 30
Schneider R., Ferrara A., Salvaterra R., Omukai K., Bromm V., 2003, Nat, 422, 869
Schneider R., Ferrara A., Salvaterra R., 2004, MNRAS, 351, 1379
Schneider R., Omukai K., Inoue A. K., Ferrara A., 2006, MNRAS, 369, 1437
Smith B. D., Sigurdsson S., Abel T., 2008, MNRAS, 385, 1443
Smith B. D., Turk M. J., Sigurdsson S., O'Shea B. W., Norman M. L., 2009, ApJ, 691, 441
Tielens A. G. G. M., Hollenbach D. J., 1985, ApJ, 291, 722
Todini P., Ferrara A., 2001, MNRAS, 325, 726
Tsuribe T., Omukai K., 2006, ApJ, 642, 61
Tumlinson J., 2007, ApJ, 664, L63
Yoshida N., Omukai K., Hernquist L., 2008, Sci, 321, 669

This paper has been typeset from a TEX/LATEX file prepared by the author.